Dominic W. Hayward, Germinal Magro, Anja Hörmann, Sylvain Prévost,
Ralf Schweins, Robert M. Richardson, Michael Gradzielski

A temperature-controlled electric field sample environment for small-angle neutron scattering experiments

Review of Scientific Instruments

A temperature-controlled electric field sample environment for small-angle neutron scattering experiments

Cite as: Rev. Sci. Instrum. **92**, 033903 (2021); https://doi.org/10.1063/5.0040675
Submitted: 15 December 2020 . Accepted: 16 February 2021 . Published Online: 08 March 2021

Dominic W. Hayward, Germinal Magro, Anja Hörmann, Sylvain Prévost, Ralf Schweins, Robert M. Richardson, and Michael Gradzielski

Review of Scientific Instruments ARTICLE scitation.org/journal/rsi

A temperature-controlled electric field sample environment for small-angle neutron scattering experiments

Cite as: Rev. Sci. Instrum. 92, 033903 (2021); doi: 10.1063/5.0040675
Submitted: 15 December 2020 • Accepted: 16 February 2021 •
Published Online: 8 March 2021

Dominic W. Hayward,[1,2,3,a] Germinal Magro,[4] Anja Hörmann,[1] Sylvain Prévost,[2] Ralf Schweins,[2] Robert M. Richardson,[4] and Michael Gradzielski[1]

AFFILIATIONS

[1] Stranski-Laboratorium für Physikalische und Theoretische Chemie, Institut für Chemie, Technische Universität Berlin, Straße des 17. Juni 124, D-10623 Berlin, Germany
[2] Institut Laue-Langevin, 71 Avenue des Martyrs, F-38042 Grenoble Cedex 9, France
[3] Jülich Centre for Neutron Science JCNS, Forschungszentrum Jülich GmbH, Outstation at MLZ, Lichtenbergstraße 1, D-85747 Garching, Germany
[4] School of Physics, University of Bristol, Tyndall Avenue, BS8 1TL Bristol, United Kingdom

[a] **Author to whom correspondence should be addressed:** d.hayward@fz-juelich.de

ABSTRACT

A new sample environment is introduced for the study of soft matter samples in electric fields using small-angle neutron scattering instruments. The sample environment is temperature controlled and features external electrodes, allowing standard quartz cuvettes to be used and conducting samples or samples containing ions to be investigated without the risk of electrochemical reactions occurring at the electrodes. For standard 12.5 mm quartz cuvettes, the maximum applied field is 8 kV/cm, and the applied field may be static or alternating (up to 10 kHz for 8 kV/cm and up to 60 kHz for 4 kV/cm). The electric fields within the sample are calculated and simulated under a number of different conditions, and the capabilities of the setup are demonstrated using a variety of liquid crystalline samples. Measurements were performed as a function of temperature and time spent in the electric field. Finally, the advantages, drawbacks, and potential optimization of the sample environment are discussed with reference to applications in the fields of complex soft matter, biology, and electrorheology.

I. INTRODUCTION

External electric fields are a very useful tool for manipulating matter from the molecular to the micrometer scale. The principle is simple: a dipole in an electric field experiences a torque that acts to orient that dipole along the direction of the field. On a molecular level, this effect has long been exploited in the form of the now ubiquitous liquid crystal display.[1,2] At larger length scales, electric fields are increasingly being used to direct the self-assembly of nanometer- to micrometer-sized building blocks to form anisotropic materials with useful photonic,[3–5] structural,[6,7] and transport properties.[8] Such a field-directed self-assembly has also been demonstrated with geometrically isotropic structures.[9] In a similar manner, they can also be used to tune the phase behavior or manipulate the internal structure of more dynamic colloidal structures.[10–12] Finally, alongside magnetic fields, electric fields are also routinely employed to modify the rheological properties (electrorheology) of certain liquids and suspensions[13–15] and to remotely power and direct the motion of microscopic "swimmers" in aqueous suspension.[16]

Given the wide range of existing and potential applications and the extensive ongoing research interest in this area, it is important to have an equally broad range of characterization techniques to study such systems. Typically, characterization techniques for the material systems outlined above include confocal laser scanning microscopy, scanning electron microscopy, and *in situ* small-angle x-ray scattering (SAXS). The latter is particularly useful, as it simultaneously provides information on the structures, interactions, and, crucially, orientations present on the nanoscale. *In situ* electric field SAXS measurements are often used to extract order parameters for oriented samples[17–19] and can provide precise

information on the orientation of the unit cell for nanocrystals[20] and lyotropic liquid-crystalline phases.[4] In liquid-crystal composite systems, where anisotropic nanoparticles with particular intrinsic properties are combined with molecular liquid crystals to modify or enhance their properties, *in situ* SAXS can be used to determine the relative orientations of the guest particles to the director of the host.[21–23]

From the numerous examples given above, it can be seen that the combination of small-angle scattering with *in situ* electric fields is a well-used technique that provides quantitative results with high information content. However, although x-ray scattering is an appropriate and convenient technique for many material systems, this is not always the case. First, the contrast in a SAXS experiment is dictated by the differences in electron density of the various components. For organic materials, these differences are rather small, and consequently, the contrast is low and difficult to model accurately. Second, organic materials can become damaged by high intensity x-rays, leaving their structure or chemistry irreversibly altered.[24] These issues may be circumvented by using neutrons instead of x rays. Neutron scattering lengths vary non-systematically over the lighter elements, leading to improved contrast conditions. This is particularly useful when investigating complex aqueous or organic systems consisting of multiple distinct populations of colloids, or a single colloid consisting of multiple components, as contrast variation and contrast matching allow each population or constituent to be studied independently.[25] Furthermore, the neutrons used in SANS experiments have relatively low kinetic energies (~10 meV) and interact overwhelmingly with nuclei rather than electrons. This means that sensitive or fragile samples may be continuously observed over the extended periods required for experiments where parameters of the electric field are varied without the risk of radiation damage.[26–28] However, despite these advantages, only a handful of such experiments featuring the combination of *in situ* electric fields and small-angle neutron scattering measurements have been reported in the literature.[8,15,29–34]

The relative lack of *in situ* SANS experiments is most likely due to a combination of the absence of lab-based neutron sources and the fact that the beam dimensions are approximately an order of magnitude larger for neutrons than for x-rays. As the electric field is inversely proportional to the distance between the electrodes, this means that much higher voltages are required to produce the same field in a SANS experiment than in an analogous SAXS setup. In all the experiments cited above, this issue was mitigated by placing the electrodes directly in contact with the sample, in some cases, simply by inserting two conducting tubes or wires into a quartz cuvette.[29,30,33,34] This method can work well for inert, insulating materials but, in samples that contain ionic or conducting components, can lead to unwanted electrochemical and resistive heating effects. To the best of our knowledge, no SANS electric field sample environments have been published with external electrodes and only two setups allowed control of the sample temperature.[8,34]

In this work, we report on the development and characterization of a "universal" electric field sample environment—one that is simple and safe, permits the use of standard cuvettes and high field strengths, and allows for temperature control. The capabilities are demonstrated using three types of sample: a thermotropic liquid crystal, a lyotropic liquid crystal, and a liquid crystal composite. The two former materials are well-known and well-studied; however, the latter is still a topic of active research.[35,36] Despite their relative abundance, ease of synthesis, and low cost, suspensions of anisotropic organic or biological nanoparticles in liquid crystals are virtually unexplored. The synthetic polypeptide, poly(γ-benzyl-L-glutamate) (PBLG), appears to be a particularly promising candidate due to its rigid α-helical structure, which results in a significant overall dipole moment (3.5 D per monomer) oriented along the backbone of the helix.[37] Here, we use PBLG, functionalized with short polyethylene glycol chains, as the anisotropic guest molecule and fully deuterated 4-cyano-4′-pentylbiphenyl (d-5CB) as the thermotropic host. Initial x-ray scattering measurements of the composite system in the nematic phase were inconclusive,[38] and it could not be determined whether the absence of x-ray scattering was due to poor solubility or insufficient scattering length density contrast. The small molecule/organic dopant liquid crystal composite system therefore represents an ideal test case for the electric field sample environment. In the following, the experimental setup will be introduced in detail and the experimental results from the thermotropic, lyotropic, and composite liquid crystal systems will be shown and discussed.

II. THE APPARATUS

A. An overview

Schematic and cross-sectional views of the electric-field sample environment are given in Fig. 1. The dimensions of the cell are 50 × 30 × 70 mm^3 (width × depth × height), and the body was constructed as a single piece by stereolithography rapid prototyping (printer—Freeform Pico two HD, Asiga, Australia, and resin—Formlabs Clear and Formlabs Gray, Formlabs, USA). Not shown in Fig. 1 is the boron carbide shielding that covers the cell body on the side facing the incoming neutron beam. The shielding is required to avoid irradiation of the electrodes and the cell body. The body features a large continuous internal cavity that can be connected to an external water bath. The cavity accounts for over a third of the total enclosed volume, ensuring that temperature changes are rapid and uniform. Although the working temperature range of the water bath was −35 °C–150 °C, the apparatus was only tested in the range 10 °C–60 °C. Lower temperatures should also be achievable using an appropriate cooling fluid; however, as the resin begins to soften at temperatures above 60 °C, higher temperatures would require the use of a different material. Temperature control is further aided by a flow of compressed air that runs in spiral-form close to the cavity walls and is then directed over the sample. In addition to assisting with the temperature homogenization, the air flow also serves to eliminate condensation at low temperatures. In situations where very high fields are required, the compressed air may be substituted with a dielectric gas, such as sulfur hexafluoride, with a high breakdown voltage to prevent unwanted and potentially dangerous arcing. The sample itself is contained in a standard rectangular quartz cuvette with a 1 mm path length (a sample environment that accepts 2 mm path length cuvettes was also fabricated). The electric field, which may be either static or dynamic, is produced using a function generator (33512B, Keysight Technologies, USA) and amplified using a high-voltage amplifier (10/10B-HS, Trek, USA). Both the input and output (via a low-level voltage signal from the amplifier) are monitored using a digital oscilloscope (TBS1000C,

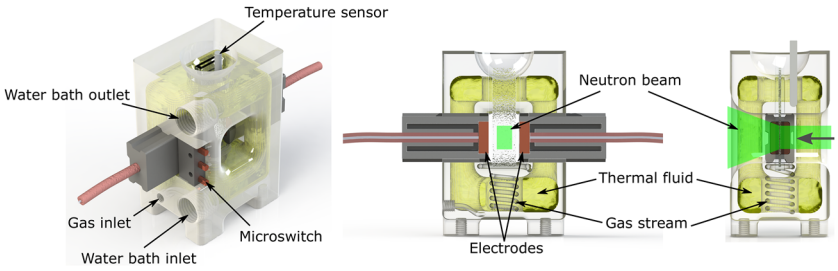

FIG. 1. Schematics produced from the .STL file used to print the sample environment. From left to right: perspective view, vertical cross section parallel to beam, and vertical cross section perpendicular to beam.

Tektronix, USA). Due to the potential dangers of working with high voltage electronics, a microswitch (see Fig. 1) that engages with the live electrode is included to ensure that the field can only be switched on when the electrode is in position.

B. Electric field simulations

In simplified 1D geometry of a dielectric sample in a quartz cuvette between two parallel conducting electrodes (as shown in Fig. 2), the electric potential is given by

$$\Delta V = -\int \vec{E} d\vec{l}. \tag{1}$$

Applying this to a filled quartz cuvette between two electrodes,

$$\begin{aligned} \Delta V &= -2E_1 l_1 - E_2 l_2 \\ &= -2\frac{E_0}{\varepsilon_1} l_1 - \frac{E_0}{\varepsilon_2} l_2, \end{aligned} \tag{2}$$

where E_0 is the field in free space, ε_1 is the dielectric constant of the quartz, l_1 is the wall thickness, ε_2 is the dielectric constant of the sample, and l_2 is the width of the sample. As the potential between the electrodes is known, Eq. (2) can be rearranged to give the E_2, the electric field in the sample,

$$E_2 = \frac{-\varepsilon_1 \Delta V}{2 l_1 \varepsilon_2 + l_2 \varepsilon_1}. \tag{3}$$

As the geometry of the sample environment is somewhat more complicated than this 1D representation, a finite element analysis (FEA) model of the sample environment was constructed and simulations were performed with the software program *ANSYS Maxwell* to determine the magnitude and geometry of the electric field within various samples. Two important effects were investigated: the influence of the dielectric constant of the sample on the magnitude of the field and the possible effects of the circulating bath fluid on the geometry of the field. The former was examined by varying the dielectric constant of the material inside the cuvette and the latter by setting the bath fluid to be either insulating or earthed (i.e., with a potential equal to zero).

Representative results are shown in Fig. S1 of the supplementary material and summarized in Table I. Despite the highly simplified nature of Eq. (3), it appears that it provides a reasonable estimate of the field strength within the sample (± ~ 20%) for most solvents. In the case of water-based solvents, however, the discrepancy between the 1D calculation and the simulations is much larger. This discrepancy arises as the 1D calculation neglects the effects of the cuvette walls on either side of the sample; when the relative differences between ε_1 and ε_2 are large, this becomes a significant source of error.

A further important finding of the FEA simulations is the influence of the thermal bath fluid on the electric field. The ethylene glycol-based thermal fluid used in this work has potentially non-negligible conductivity (σ ~ 5 mS/cm, cf. σ_{H_2O} ~ 0.05 μS/cm) and is in direct contact with the earthed thermal bath. The two simulations therefore probed the two extreme cases in which the fluid is either a perfect insulator or a perfect conductor. Although the difference between the electric fields at the center of the sample is minimal, the effect on the geometry of the field is much more pronounced, as shown in Figs. S1 and S2 of the supplementary material. In the case of an insulating thermal fluid, the electric field vectors are horizontal and the field strength is uniform in the region of interest (σ/μ = 0.02). A conductive thermal fluid, however, results in increased divergence of field vectors and gradient in the field strength (σ/μ = 0.1). Even in this worst case scenario, however, the

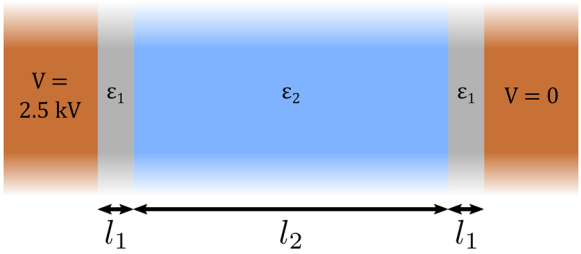

FIG. 2. Diagram of the one-dimensional geometry used to estimate the electric field strength in the sample via Eq. (3). For the Hellma 110-QS cuvettes used in this work, l_1 = 1.5 mm, l_2 = 9.5 mm, and ε_1 = 4.2.

TABLE I. Summary of the calculated/simulated electric fields present at the center of the neutron beam for an applied voltage of 2.5 kV. Equation (3) refers to the field strengths calculated via Eq. (3) in the text, Sim. 1 refers to the FEA simulation in which the bath fluid is an insulator, and Sim. 2 corresponds to the FEA simulation in which the bath fluid is an earthed conductor.

Sample	Dielectric Constant	Field in Sample (kV/cm)		
		Equation (3)	Sim. 1	Sim. 2
Dioxane	2.25	2.3	1.9	1.8
5CB (isotropic)	11.2	1.6	1.7	1.6
5CB (oriented)	19.7	1.2	1.5	1.3
Water	80	0.46	0.8	0.75

electric field appears to be sufficiently horizontal and uniform to perform field-alignment experiments.

Finally, the field strengths attained in the region of interest of the sample are on the order of 1 kV/cm–2 kV/cm. This compares favorably with the previous SANS electric field sample environments, even those with immersed electrodes. Furthermore, as the amplifier used in this experiment has the capacity for a sustained output of 10 kV, the maximum field strengths in the sample may be increased by a factor of 4 compared to the values provided in Table I. Although the breakdown voltage of dry air is 30 kV/cm, environmental factors such as increased humidity and air pressure may reduce this,[40] leading to potentially dangerous arcing between the electrodes. If such high field strengths are required, care should be taken that all the components are clean and dry and that no condensation forms on the cuvette.

III. RESULTS

A. Experimental details

1. Materials

Unless otherwise stated, all chemicals were purchased from Sigma Aldrich (St. Louis, USA) and used without further purification. The PBLG material (15 kDa–70 kDa) was purchased from Santa Cruz Biotechnology (Santa Cruz, USA). Deuterated 1,4-dioxane (>99% atom D) was purchased from abcr (Karlsruhe, Germany), and the perdeuterated 4-cyano-4′-pentylbiphenyl liquid crystal (d-5CB) was synthesized by the Zimmermann group at the Max Planck Institute for Medical Research in Heidelberg. Hydrogenous 4-cyano-4′-octylbiphenyl (8CB) was purchased from Kingston Chemicals, Ltd. (Hull, UK). The structural formulas of d-5CB and 8CB are shown in Fig. S3 of the supplementary material. The deionized water used for dialysis was taken from a Milli-Q Reference water purification system with a resistivity of ~18 MΩ cm.

2. Sample synthesis and preparation

The grafting reaction was conducted following a standard transesterification procedure,[41–43] whereby benzyl groups are exchanged with short PEG chains in the presence of an acidic catalyst. The reaction was carried out using Schlenk techniques under an atmosphere of nitrogen. The PBLG (1.3 g, 0.074 mmol, and 5.6 mmol BLG residues) and mPEG (M_w of 350 Da, 35 ml, and 109 mmol) were added to a Schlenk flask and dried under vacuum at 40 °C for 1 h. The reagents were then dissolved in dry 1,2-dichloroethane (99.8%, 70 ml) and the *p*-toluenesulfonic acid catalyst (5.2 g, 27.3 mmol) was added in one portion. The reaction mixture was stirred, heated to 64 °C, and the reaction was allowed to proceed at that temperature for 5 days. The polymer solution was then cooled to room temperature and opened to air and the solvent was evaporated until the volume had approximately halved. The mixture was then transferred to dialysis tubing (*Snakeskin* 3.5 kDa molecular weight cutoff, Fisher scientific) and was dialyzed against stirring deionized (DI) water (~1 l) for further seven days during which time a pale yellow paste-like sediment formed. The DI water was exchanged every day to ensure complete removal of any remaining organic solvents, mPEG and *p*-toluenesulfonic acid. The product was extracted into dichloromethane and the resulting solution was evaporated and then dried under vacuum, yielding a pale yellow viscous wax-like substance in quantitative yield. The structural formula of the PEGylated PBLG is given in Fig. S3(c) of the supplementary material.

Guest-host liquid crystal samples were prepared at 2 wt. % by dissolving a known mass of PEGylated PBLG in chloroform, adding the solution to the appropriate mass of the d-5CB liquid crystal, and vortexing the mixture. The mixtures were then placed in a vacuum oven for 16 h at 40 °C under a static vacuum (~10 mbar), allowing the chloroform to evaporate. The samples were transferred into pre-heated cuvettes at 40 °C and placed directly into the sample environment immediately prior to measurement (also at a set temperature of 40 °C).

3. SANS

SANS measurements were conducted on the D11 instrument at the ILL (Grenoble, France) and the Sans2d time-of-flight instrument at ISIS (Harwell, UK). Measurements of the hydrogenous 8CB were performed on D11 with a sample-to-detector distance of 1.4 m and collimation length of 8 m. For measurements of the lyotropic and guest–host liquid crystals performed on D11, three sample-to-detector distances were used (1.4 m, 8 m, and 39 m, with collimation lengths of 8 m, 8 m, and 39 m, respectively) with a wavelength of 6 Å, giving a Q-range of 0.0015 $Å^{-1}$–0.42 $Å^{-1}$. Measurements on Sans2d were performed with a sample to (rear) detector distance of 4 m, giving a Q-range of 0.0062 $Å^{-1}$–0.96 $Å^{-1}$. All measurements were performed in 1 mm path length cuvettes and, unless otherwise specified, samples were measured at 25 °C, as recorded by the thermocouple directly adjacent to the sample.

B. Thermotropic liquid crystal

In order to confirm that the sample environment was functioning as intended, the first sample to be tested was the hydrogeneous liquid crystal, 8CB. The solid to smectic-A, smectic-A to nematic, and nematic to isotropic phase transitions for 8CB occur at the T_{KA} of 22 °C, T_{NA} of 34 °C, and T_{NI} of 41 °C, respectively.[39] The sample was therefore heated to 45 °C and cooled at a rate of 1.5 °C/min to 20 °C. For the duration of the experiment, an alternating potential of 2 kV was applied across the sample (i.e., an effective maximum field of ~1.2 kV/cm within the sample) at a frequency of 1 kHz. The scattering was measured in 30 s intervals, and the results are given in Fig. 3. The temperature control and application of the electric field clearly have the desired effects, with transitions and alignment of the smectic/crystalline phases occurring as expected, confirming that the sample environment is fully functional.

C. Lyotropic liquid crystal

A second experiment was performed at a constant temperature of 25 °C in order to observe the slow orientation of lyotropic suspensions of unadulterated PBLG helices (10 wt. %) in deuterated dioxane. Again, an alternating electric field of 2 kV was applied across the sample (i.e., an effective maximum field of ~1.4 kV/cm within the sample) at a frequency of 1 kHz. The scattering was measured in 60 s intervals and the results are shown in Fig. 4. It can be seen that the alignment of the mesophasic domains occurs on a much longer timescale than in the case of thermotropic liquid crystals. The degree

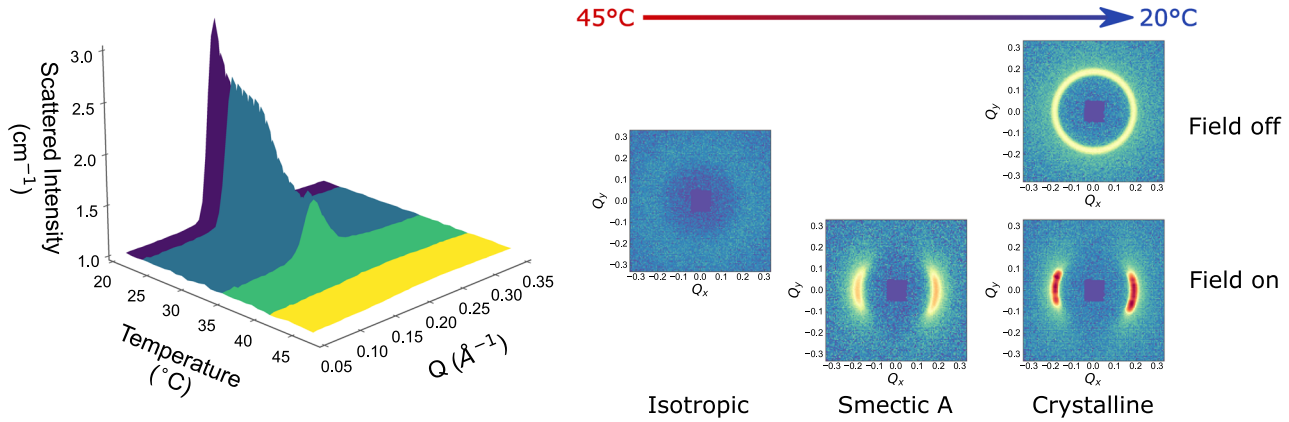

FIG. 3. Left: azimuthally averaged SANS data as a function of temperature for hydrogenous 8CB cooling in an electric field. Right: detector images showing the different liquid crystalline phases in the presence or absence of an electric field (data are not normalized but are all shown on the same intensity scale). Initially, at 45 °C, the 8CB is in the isotropic phase (shown here in yellow). On cooling, a broad peak appears in the nematic phase (light green), which sharpens at ~35 °C at the transition to the smectic phase (dark green). On further cooling in the smectic phase, the peak intensity increases until the onset of crystallization (purple) at ~22 °C. The color transitions shown here correspond to the known liquid crystalline transition temperatures.[39]

of alignment can be quantified by comparing the alignment of individual mesogens (in this case, the PBLG helices) with that of the director to determine an orientational distribution function, $f(\theta)$, and averaging over the ensemble. By convention, this is often given by the average of the second Legendre polynomial, P_2,

$$S = \langle P_2(\cos\theta)\rangle = \left\langle \frac{3}{2}\cos^2\theta - \frac{1}{2}\right\rangle, \tag{4}$$

where S is the order parameter, θ is the angle between the long axis of the molecule and the director, and the angle brackets denote the ensemble average such that

$$S = \frac{\int_0^\pi f(\theta)\left(\frac{3}{2}\cos^2\theta - \frac{1}{2}\right)\sin\theta\,d\theta}{\int_0^\pi f(\theta)\sin\theta\,d\theta}. \tag{5}$$

The order parameter varies between $S = 1$ when all of the mesogens are perfectly aligned with the director [i.e., $f(\theta) = \delta(0)$] and $S = 0$ when the orientation is perfectly isotropic [i.e., $f(\theta)$ is a constant and there is no orientational order at all]. The evolution of the scattering, the corresponding order parameter, and the final detector image are shown in Fig. 4. Using the framework developed by Wagner[44] for liquid crystals in magnetic fields, this information can be used to determine the texture viscosity of the mesophase,

$$\eta = \frac{\varepsilon_0\chi_e E^2}{6\beta}, \tag{6}$$

where ε_0 is the permittivity of free space, χ_e is the dielectric susceptibility of PBLG in dioxane, E is the electric field strength, and β, a prefactor that arises when evaluating the complex viscoelastic response of lyotropic liquid crystals,[44] is the governed by the equation

$$\ln\left(\frac{\sqrt{\frac{1}{2}} + \frac{S}{\sqrt{5}}}{\sqrt{\frac{1}{2}} - S}\right) = \frac{4}{3}\beta t \tag{7}$$

and can be determined from the linear gradient of the left-hand side of Eq. (7) plotted against time. As shown in the plot in Fig. S4 of the supplementary material, the evolution of the left-hand side of Eq. (7) is linear with time, yielding a value of $\beta = 1.25 \times 10^{-4}$ s^{-1}. According

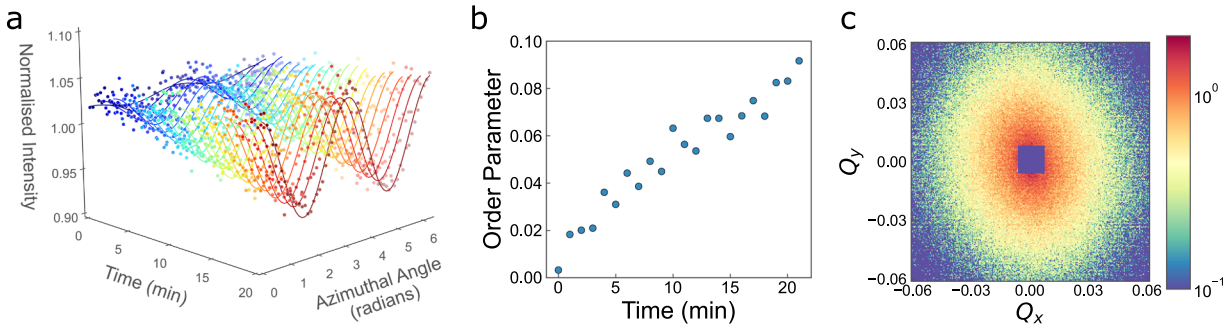

FIG. 4. (a) Time-resolved, radially averaged and normalized SANS data of unadulterated PBLG helices (10 wt. %) in deuterated dioxane aligning in an electric field at 25 °C, (b) the corresponding order parameter, and (c) the final detector image after 20 min.

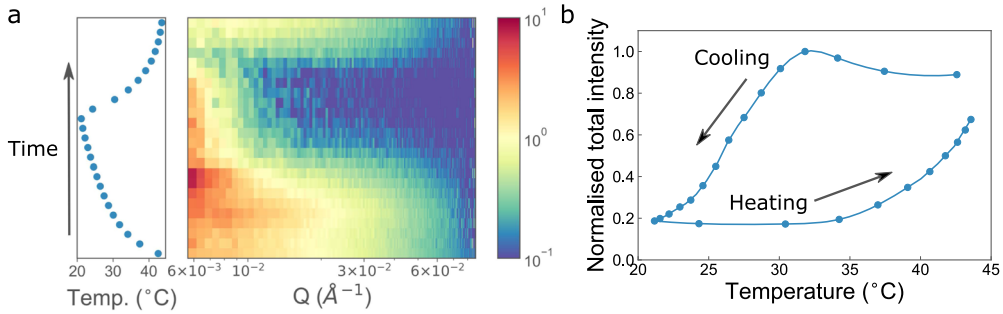

FIG. 5. (a) Temperature (left) and the corresponding azimuthally averaged SANS data (right) showing the initial increase in intensity at low Q, followed by the rapid decline in intensity at higher Q as the temperature is decreased and finally an increase in intensity at higher Q with the increase in temperature, corresponding to aggregation, precipitation, and re-dissolution, respectively. (b) The time-averaged integrated total detector intensity (i.e., total counts on the detector per unit time) as a function of temperature.

to dielectric studies of PBLG in various solvents, the relative permittivity of the lyotropic suspension is approximately a factor of two higher than that of the pure solvent.[45] Equation (6) yields a texture viscosity of 800 Pa s. This is more than an order of magnitude higher than that found by Wagner *et al.* (28 Pa s) for PBLG helices in DMF-d7. The reasons for this discrepancy are unclear; however, it is known that low dielectric solvents such as dioxane give rise to extensive aggregation of PBLG helices,[46–48] leading to an increase in viscosity.[49] It is conceivable that the field inhomogeneity, as observed in Fig. S1, also plays a role in depressing the calculated order parameter. However, the same calculation yields a value of $S = 0.80$ for the smectic A phase of the thermotropic 8CB liquid crystal, which is in line with other theoretical and experimental observations of similar compounds.[50–53] The field inhomogeneity is therefore unlikely to be the cause of the anomalously high texture viscosity. In light of these intriguing preliminary results, further orientational order parameter studies with different solvents and mesogens are required to fully explain this phenomenon.

D. Guest–host liquid crystal

The electric field sample environment is also ideally suited to investigating the properties of guest–host liquid crystal systems. In this study, modified PEGylated PBLG helices were introduced (2 wt. %) into the deuterated form of the liquid crystal, 4-cyano-4′-pentylbiphenyl (d-5CB), and the samples were measured as they were cooled from the isotropic phase to the nematic phase in the presence of an alternating applied electric field (5 kV_{pp}, 1 kHz). It was observed that the modified PBLG material is well-dissolved and retains its rod-like character in the isotropic phase, as can be seen from the Q^{-1} dependence of the scattering in the Guinier region (see Fig. S5 of the supplementary material). There is some evidence of aggregation, as illustrated by the slight upturn at low Q, but this is less pronounced than for the same PEGylated PBLG material in d-dioxane. Fitting the data to a model for randomly oriented cylinders using the SasView application (see Table S1) revealed that the PEGylated PBLG has a larger cross-sectional radius than the unadulterated material (14 Å vs 10 Å), presumably due to the longer side chains. The fits also suggest that helices are longer in the liquid crystal than in dioxane, and this could be evidence of end-to-end aggregation; however, due to the divergence of the data to the fits at low Q, this is not necessarily significant.

Despite the good solubility in the isotropic phase, on cooling below the isotropic nematic transition temperature, the PBLG material begins to precipitate out of the nematic phase. This behavior can clearly be seen in Fig. 5; as the temperature decreases, the intensity initially increases at low Q, presumably due to the formation of larger aggregates before the intensity drops off substantially at high Q. Once the temperature increases above the nematic-to-isotropic transition, the intensity at high Q begins to recover as the helices are gradually "redissolved" in the liquid crystal. The changes can also be observed in the detector images shown in Fig. S6(a) in the supplementary material. At T = 30 °C, the intensity of the scattering close to the beamstop increases and becomes isotropic (the intensity is higher above and below the beamstop), indicating the presence of large horizontally aligned aggregates. Indeed, when the sample is removed from the electric field, these aggregates are visible to the naked eye as streaks on the walls of the cuvette, radiating out from the electrode [see Fig. S6(b)]. The large surface area of the PBLG aggregate film on the cuvette walls also explains the comparatively fast "redissolution" of the helices into the composite upon heating.

These results indicate that, although the PEGylated polypeptides are well-solvated and maintain the α-helical structure in the isotropic phase, they are excluded from solution during the isotropic–nematic transition. It is considered likely that this aggregation behavior may be due to the influence of the nematic field, whereby colloidal particles are effectively bound together by disclinations anchored to their surface.[54] Although these results resolve the question surrounding the absence of particle scattering in the x-ray measurements, they unfortunately also preclude further investigation on the influence of temperature, field strength, and frequency on the guest–host system that would otherwise have been possible using this sample environment.

IV. DISCUSSION AND CONCLUSIONS

Conceived to counteract the relative dearth in electric field sample environments available to users of SANS instruments, the setup described herein was designed to be as functional, flexible, and user friendly as possible. It features external electrodes, allowing potentially conducting samples to be studied, accepts standard

quartz cuvettes, and allows for fields up to 8 kV/cm to be applied to the sample. Furthermore, the temperature can be controlled by means of a standard water bath and the air flow around the sample ensures a uniform temperature and mitigates the potential problem of condensation at low temperatures. Finally, the setup is easy to assemble and the sample holder itself can be 3D-printed on any suitable printer. The temperature, field-strength, and frequency can all be controlled remotely via the instrument control software.

Commissioning experiments were conducted on thermotropic, lyotropic, and guest–host liquid crystal systems. It was shown that the sample environment functions as expected and can be used to investigate various alignment phenomena. However, due to the aggregation of guest molecules in the nematic phase, the effects of field-strength and frequency could not be explored to their full extent. In addition to the types of liquid crystalline system exhibited in this work, the electric field sample environment is well-suited to study a wide variety of field-alignable and electro-responsive systems, including organic[55] and inorganic nanoparticles,[21] biological structures,[56] and directed self-assembly systems,[57] and can be used to complement magnetic-field alignment experiments. Furthermore, the use of the high-speed high-voltage amplifier allows alternating fields with frequencies up to ~60 kHz to be applied, and the sample environment is therefore well-suited to stroboscopic techniques such as TISANE,[58,59] enabling alignment or relaxation phenomena to be investigated on millisecond timescales.

The principal drawbacks of the design presented here are the limit of the maximum temperature due to the properties of the resin and the inhomogeneity of the field in the presence of a conducting thermal fluid. The first issue can easily be solved by fabricating the sample holder from a ceramic material, which is both electrically insulating and thermally conducting, thereby increasing the temperature range and decreasing the equilibration time. The inhomogeneity in the field can be somewhat mitigated by using deionized water or oil-based fluids instead of ethylene glycol. However, this will not completely eliminate the problem as ions will rapidly leach into the thermal fluid from the water bath, increasing the conductivity. A more complete solution would be to apply a symmetrical field with two live electrodes driven in anti-phase and to replace the thermal fluid with a temperature-controlled air flow over the sample, which also has the advantage of facilitating rapid temperature jumps. The sample environment is currently available to users at the ILL neutron scattering facility and the .STL file is available from the authors on request.

SUPPLEMENTARY MATERIAL

See the supplementary material for figures S1–S6 and Table S1 referenced in the text.

ACKNOWLEDGMENTS

This work was funded by the BMBF (Grant No. 05K16KT1). Experiments at the ISIS Neutron and Muon Source were supported by a beamtime allocation No. RB1520013 from the Science and Technology Facilities Council. The authors gratefully acknowledge Herbert Zimmerman for providing us with the perdeuterated liquid crystal and the ILL Instrument Control Service for their support before and during the experiment and thank Frédéric Thomas at the ILL for running the FEA simulations featured in this work. D.W.H. also thanks the Partnership for Soft Condensed Matter (PSCM) and, particularly, Peter van der Linden, Diego Pontoni, and Yuri Gerelli for their helpful advice and use of the rapid prototyping facility. This work benefited from the use of the SasView application, originally developed under NSF Award No. DMR-0520547. SasView contains the code developed with funding from the European Union's Horizon 2020 research and innovation programme under the SINE2020 project (Grant Agreement No. 654000).

DATA AVAILABILITY

The data that support the findings of this study will be made openly available in the ILL data repository at http://doi.org/10.5291/ILL-DATA.9-11-1857 shortly after publication.[60] In the meantime, the data are available from the corresponding author upon reasonable request.

REFERENCES

[1] R. Williams, "Domains in liquid crystals," J. Chem. Phys. **39**, 384–388 (1963).
[2] G. H. Heilmeier, "Liquid crystal displays: An experiment in interdisciplinary research that worked," IEEE Trans. Electron Devices **23**, 780–785 (1976).
[3] T. Gong, D. T. Wu, and D. W. M. Marr, "Electric field-reversible three-dimensional colloidal crystals," Langmuir **19**, 5967–5970 (2003).
[4] E. Paineau, M. E. M. Krapf, M. S. Amara, N. V. Matskova, I. Dozov, S. Rouzière, A. Thill, P. Launois, and P. Davidson, "A liquid-crystalline hexagonal columnar phase in highly-dilute suspensions of imogolite nanotubes," Nat. Commun. **7**, 10271 (2016).
[5] E. V. Yakovlev, K. A. Komarov, K. I. Zaytsev, N. P. Kryuchkov, K. I. Koshelev, A. K. Zotov, D. A. Shelestov, V. L. Tolstoguzov, V. N. Kurlov, A. V. Ivlev, and S. O. Yurchenko, "Tunable two-dimensional assembly of colloidal particles in rotating electric fields," Sci. Rep. **7**, 13727 (2017).
[6] M. Mittal and E. M. Furst, "Electric field-directed convective assembly of ellipsoidal colloidal particles to create optically and mechanically anisotropic thin films," Adv. Funct. Mater. **19**, 3271–3278 (2009).
[7] S. Nöjd, P. S. Mohanty, P. Bagheri, A. Yethiraj, and P. Schurtenberger, "Electric field driven self-assembly of ionic microgels," Soft Matter **9**, 9199–9207 (2013).
[8] Y. Xi and L. D. Pozzo, "Electric field directed formation of aligned conjugated polymer fibers," Soft Matter **13**, 3894–3908 (2017).
[9] B. Bharti and O. D. Velev, "Assembly of reconfigurable colloidal structures by multidirectional field-induced interactions," Langmuir **31**, 7897–7908 (2015).
[10] A. Yethiraj and A. van Blaaderen, "A colloidal model system with an interaction tunable from hard sphere to soft and dipolar," Nature **421**, 513–517 (2003).
[11] A. A. Shah, B. Schultz, W. Zhang, S. C. Glotzer, and M. J. Solomon, "Actuation of shape-memory colloidal fibres of Janus ellipsoids," Nat. Mater. **14**, 117–124 (2014).
[12] T. Colla, P. S. Mohanty, S. Nöjd, E. Bialik, A. Riede, P. Schurtenberger, and C. N. Likos, "Self-assembly of ionic microgels driven by an alternating electric field: Theory, simulations, and experiments," ACS Nano **12**, 4321–4337 (2018).
[13] T. C. Halsey, "Electrorheological fluids," Science **258**, 761–766 (1992).
[14] M. T. Cidade, G. Pereira, A. Bubnov, V. Hamplova, M. Kaspar, and J. P. Casquilho, "Rheological characterisation of a liquid-crystalline diol and its dependence with an applied electric field," Liq. Cryst. **39**, 191–197 (2012).
[15] R. Tao, E. Du, H. Tang, and X. Xu, "Neutron scattering studies of crude oil viscosity reduction with electric field," Fuel **134**, 493–498 (2014).
[16] J. Roche, S. Carrara, J. Sanchez, J. Lannelongue, G. Loget, L. Bouffier, P. Fischer, and A. Kuhn, "Wireless powering of *e* -swimmers," Sci. Rep. **4**, 6705 (2015).
[17] E. Paineau, I. Dozov, A.-M. Philippe, I. Bihannic, F. Meneau, C. Baravian, L. J. Michot, and P. Davidson, "In-situ SAXS study of aqueous clay suspensions submitted to alternating current electric fields," J. Phys. Chem. B **116**, 13516–13524 (2012).

[18]J. B. Gilroy, P. A. Rupar, G. R. Whittell, L. Chabanne, N. J. Terrill, M. A. Winnik, I. Manners, and R. M. Richardson, "Probing the structure of the crystalline core of field-aligned, monodisperse, cylindrical polyisoprene-block-polyferrocenylsilane micelles in solution using synchrotron small- and wide-angle X-ray scattering," J. Am. Chem. Soc. **133**, 17056–17062 (2011).
[19]D. W. Hayward, J. B. Gilroy, P. A. Rupar, L. Chabanne, C. Pizzey, M. A. Winnik, G. R. Whittell, I. Manners, and R. M. Richardson, "Liquid crystalline phase behavior of well-defined cylindrical block copolymer micelles using synchrotron small-angle X-ray scattering," Macromolecules **48**, 1579–1591 (2015).
[20]Y. Yu, D. Yu, B. Sadigh, and C. A. Orme, "Space- and time-resolved small angle X-ray scattering to probe assembly of silver nanocrystal superlattices," Nat. Commun. **9**, 4211 (2018).
[21]R. J. Greasty, R. M. Richardson, S. Klein, D. Cherns, M. R. Thomas, C. Pizzey, N. Terrill, and C. Rochas, "Electro-induced orientational ordering of anisotropic pigment nanoparticles," Philos. Trans. R. Soc., A **371**, 20120257 (2013).
[22]J. E. Hallett, D. W. Hayward, P. Bartlett, and R. M. Richardson, "A small-angle X-ray scattering study of nanoparticle assembly in an aligned nematic liquid crystal," Liq. Cryst. **41**, 1791–1802 (2014).
[23]M. R. Thomas, J. E. Hallett, S. Klein, S. Mann, A. W. Perriman, and R. M. Richardson, "Stability and orientational order of gold nanorods in nematic suspensions: A small angle X-ray scattering study," Mol. Cryst. Liq. Cryst. **610**, 44–50 (2015).
[24]J. C. Brooks-Bartlett, R. A. Batters, C. S. Bury, E. D. Lowe, H. M. Ginn, A. Round, and E. F. Garman, "Development of tools to automate quantitative analysis of radiation damage in SAXS experiments," J. Synchrotron Radiat. **24**, 63–72 (2017).
[25]A. Banc, C. Charbonneau, M. Dahesh, M.-S. Appavou, Z. Fu, M.-H. Morel, and L. Ramos, "Small angle neutron scattering contrast variation reveals heterogeneities of interactions in protein gels," Soft Matter **12**, 5340–5352 (2016).
[26]N. Niimura and A. Podjarny, "The basic principles and experimental configurations of neutron diffraction experiments," in *Neutron Protein Crystallography* (Oxford University Press, 2011), pp. 1–49.
[27]K.-H. Tang and R. E. Blankenship, "Neutron and light scattering studies of light-harvesting photosynthetic antenna complexes," Photosynth. Res. **111**, 205–217 (2012).
[28]B. Zhang-Haagen, R. Biehl, L. Nagel-Steger, A. Radulescu, D. Richter, and D. Willbold, "Monomeric amyloid beta peptide in hexafluoroisopropanol detected by small angle neutron scattering," PLoS One **11**, e0150267 (2016).
[29]J. Baumann, J. Kalus, G. Neubauer, H. Hoffmann, and K. Ibel, "Transient SANS Studies on p-Tetrafluorethylen (p-TFE)," Ber. Bunsengesellschaft Phys. Chem. **93**, 874–878 (1989).
[30]J. Baumann, G. Hertel, H. Hoffmann, K. Ibel, V. Jindal, J. Kalus, P. Lindner, G. Neubauer, H. Pilsl, W. Ulbricht, and U. Schmelzer, "Time-dependent small angle neutron measurements of aligned micelles," Prog. Colloid Polym. Sci. **81**, 100–106 (1990).
[31]F. C. Giacomelli, N. P. Da Silveira, F. Nallet, P. Černoch, M. Steinhart, and P. Štěpánek, "Cubic to hexagonal phase transition induced by electric field," Macromolecules **43**, 4261–4267 (2010).
[32]J. M. McMullan and N. J. Wagner, "Directed self-assembly of colloidal crystals by dielectrophoretic ordering observed with small angle neutron scattering (SANS)," Soft Matter **6**, 5443–5450 (2010).
[33]M. Rajnak, V. I. Petrenko, M. V. Avdeev, O. I. Ivankov, A. Feoktystov, B. Dolnik, J. Kurimsky, P. Kopcansky, and M. Timko, "Direct observation of electric field induced pattern formation and particle aggregation in ferrofluids," Appl. Phys. Lett. **107**, 073108 (2015).
[34]S. Nöjd, C. Hirst, M. Obiols-Rabasa, J. Schmitt, A. Radulescu, P. S. Mohanty, and P. Schurtenberger, "Soft particles in an electric field–A zero average contrast study," Soft Matter **15**, 6369–6374 (2019).
[35]H. Kim, S. H. Ryu, M. Tuchband, T. J. Shin, E. Korblova, D. M. Walba, N. A. Clark, and D. K. Yoon, "Structural transitions and guest/host complexing of liquid crystal helical nanofilaments induced by nanoconfinement," Sci. Adv. **3**, e1602102 (2017).
[36]S. K. Fegan, P. Kirsch, and F. Müller-Plathe, "The alignment of dichroic dyes in a nematic liquid crystal: A molecular dynamics investigation," Liq. Cryst. **45**, 1377–1384 (2018).
[37]B. M. Ginzburg and A. A. Shepelevskii, "Construction of the full phase diagram for the system of poly(γ-benzyl- L -glutamate)/dimethylformamide on the basis of the complex of literature data," J. Macromol. Sci., Part B: Phys. **42**, 1–56 (2003).
[38]D. N. Harris, "Liquid crystal enhancement by nanoparticle additives," M.Sc. thesis, University of Bristol, 2015.
[39]J. Thoen, H. Marynissen, and W. Van Dael, "Temperature dependence of the enthalpy and the heat capacity of the liquid-crystal octylcyanobiphenyl (8CB)," Phys. Rev. A **26**, 2886–2905 (1982).
[40]J. T. Krile, A. A. Neuber, J. C. Dickens, and H. G. Krompholz, "DC flashover of a dielectric surface in atmospheric conditions," IEEE Trans. Plasma Sci. **32**, 1828–1834 (2004).
[41]D. Tang, J. Lin, S. Lin, S. Zhang, T. Chen, and X. Tian, "Self-assembly of poly(γ-benzyl L-glutamate)-graft-poly(ethylene glycol) and its mixtures with poly(γ-benzyl L-glutamate) homopolymer," Macromol. Rapid Commun. **25**, 1241–1246 (2004).
[42]T. Li, J. Lin, T. Chen, and S. Zhang, "Polymeric micelles formed by polypeptide graft copolymer and its mixtures with polypeptide block copolymer," Polymer **47**, 4485–4489 (2006).
[43]G.-Q. Zhu, F.-G. Wang, and Y.-Y. Liu, "Effects of reaction conditions on the grafting percentage of poly(ethylene glycol)- block-poly(γ-benzyl L-glutamate)-graft-poly(ethylene glycol) copolymer," J. Braz. Chem. Soc. **21**, 715–720 (2010).
[44]N. J. Wagner and L. M. Walker, "Determination of the texture viscosity and elasticity of a nematic PBLG/d-DMF solution through magnetic field alignment," Macromolecules **27**, 5979–5986 (1994).
[45]H. Watanabe, K. Yoshioka, and A. Wada, "Electrooptical and dielectric investigations on the conformation and the electrical properties of poly-γ-benzyl-L-glutamate in mixed solvents," Biopolymers **2**, 91–101 (1964).
[46]A. K. Gupta, C. Dufour, and E. Marchal, "Structure of aggregates and helix-coil transition of polypeptides by dielectric measurements. I. Poly-γ-benzyl-L-glutamate in dioxane and dioxane-dichloroacetic acid," Biopolymers **13**, 1293–1308 (1974).
[47]A. Wada, "Dielectric properties of polypeptide solutions. V. Molecular association of the α-helix in solution," J. Polym. Sci. **45**, 145–153 (1960).
[48]R. Sakamoto and M. Watanabe, "Effects of molecular weight on the aggregation of poly-(γ-benzyl L-glutamate) in dilute solution," in *Contemporary Topics in Polymer Science* (Springer, New York, Boston, MA, 1984), pp. 259–268.
[49]J. C. Powers and W. L. Peticolas, "Electrical ordering in polypeptide solutions," in *Advances in Chemistry* (American Chemical Society, 1967), pp. 217–231.
[50]P. Davidson, D. Petermann, and A. M. Levelut, "The measurement of the nematic order parameter by X-ray scattering reconsidered," J. Phys. II **5**, 113–131 (1995).
[51]N. Bielejewska, E. Chrzumnicka, E. Mykowska, R. Przybylski, M. Szybowicz, K. Władysiak, and D. Bauman, "Comparative study of orientational order of some liquid crystals from various homologous series," Acta Phys. Pol., A **110**, 777–793 (2006).
[52]M. T. Sims, L. C. Abbott, R. M. Richardson, J. W. Goodby, and J. N. Moore, "Considerations in the determination of orientational order parameters from X-ray scattering experiments," Liq. Cryst. **46**, 11–24 (2019).
[53]Z. Zhang, V. P. Panov, M. Nagaraj, R. J. Mandle, J. W. Goodby, G. R. Luckhurst, J. C. Jones, and H. F. Gleeson, "Raman scattering studies of order parameters in liquid crystalline dimers exhibiting the nematic and twist-bend nematic phases," J. Mater. Chem. C **3**, 10007–10016 (2015).
[54]T. Araki and H. Tanaka, "Colloidal aggregation in a nematic liquid crystal: Topological arrest of particles by a single-stroke disclination line," Phys. Rev. Lett. **97**, 127801 (2006).
[55]B. Berke, O. Czakkel, L. Porcar, E. Geissler, and K. László, "Static and dynamic behaviour of responsive graphene oxide–poly(N-isopropyl acrylamide) composite gels," Soft Matter **12**, 7166–7173 (2016).
[56]K. Kang, "Charged fibrous viruses (fd) in external electric fields: Dynamics and orientational order," New J. Phys. **12**, 063017 (2010).
[57]H. U. Jeon, H. M. Jin, J. Y. Kim, S. K. Cha, J. H. Mun, K. E. Lee, J. J. Oh, T. Yun, J. S. Kim, and S. O. Kim, "Electric field directed self-assembly of block copolymers for rapid formation of large-area complex nanopatterns," Mol. Syst. Des. Eng. **2**, 560–566 (2017).
[58]D. Kipping, R. Gähler, and K. Habicht, "Small angle neutron scattering at very high time resolution: Principle and simulations of 'TISANE,'" Phys. Lett. A **372**, 1541–1546 (2008).

[59]P. Bender, A. Günther, D. Honecker, A. Wiedenmann, S. Disch, A. Tschöpe, A. Michels, and R. Birringer, "Excitation of Ni nanorod colloids in oscillating magnetic fields: A new approach for nanosensing investigated by TISANE," Nanoscale **7**, 17122–17130 (2015).

[60]D. Hayward, L. Chiappisi, M. Gradzielski, A. Hoermann, G. Magro, S. Prevost, R. M. Richardson, and R. Schweins, "Investigating the aggregation and disaggregation of polypeptide helices: A new route to stable liquid crystal composites," dataset at Institut Laue Langevin (ILL) repository (2018), http://doi.org/10.5291/ILL-DATA.9-11-1857